

## Multiband Superconductivity with Sign-Preserving Order Parameter in Kagome Superconductor CsV<sub>3</sub>Sb<sub>5</sub>

Han-Shu Xu<sup>1</sup>, Ya-Jun Yan<sup>1,\*</sup>, Ruotong Yin<sup>1</sup>, Wei Xia<sup>2,3</sup>, Shijie Fang<sup>1</sup>, Ziyuan Chen<sup>1</sup>,  
Yuanji Li<sup>1</sup>, Wenqi Yang<sup>1</sup>, Yanfeng Guo<sup>3</sup>, and Dong-Lai Feng<sup>1,4,5,†</sup>

<sup>1</sup>Hefei National Laboratory for Physical Sciences at the Microscale and Department of Physics,  
University of Science and Technology of China, Hefei 230026, China

<sup>2</sup>School of Physical Science and Technology, ShanghaiTech University, Shanghai 201210, China

<sup>3</sup>ShanghaiTech Laboratory for Topological Physics, ShanghaiTech University, Shanghai 201210, China

<sup>4</sup>Collaborative Innovation Center of Advanced Microstructures, Nanjing 210093, China

<sup>5</sup>Shanghai Research Center for Quantum Sciences, Shanghai 201315, China

 (Received 27 April 2021; revised 13 August 2021; accepted 30 September 2021; published 29 October 2021)

The superconductivity of a kagome superconductor CsV<sub>3</sub>Sb<sub>5</sub> is studied by scanning tunneling microscopy and spectroscopy at ultralow temperature with high resolution. Two kinds of superconducting gaps with multiple sets of coherent peaks and residual zero-energy density of states (DOS) are observed on both half-Cs and Sb surfaces, implying multiband superconductivity. In addition, in-gap states can be induced by magnetic impurities but not by nonmagnetic impurities, suggesting a sign-preserving or *s*-wave superconducting order parameter. Moreover, the interplay between charge density waves (CDW) and superconductivity differs on various bands, resulting in different density-of-states distributions. Our results suggest that the superconducting gap is likely isotropic on the sections of Fermi surface that play little roles in CDW, and the superconducting gaps on the sections of Fermi surface with anisotropic CDW gaps are likely anisotropic as well. The residual spectral weights at zero energy are attributed to the extremely small superconducting gap on the tiny oval Fermi pockets. Our study provides critical clues for further understanding the superconductivity and its relation to CDW in CsV<sub>3</sub>Sb<sub>5</sub>.

DOI: [10.1103/PhysRevLett.127.187004](https://doi.org/10.1103/PhysRevLett.127.187004)

Owing to the special geometry, materials with kagome lattice may possess geometric frustration, flat band and nontrivial band topology, providing an intriguing playground to explore exotic quantum phenomena, such as quantum spin liquid, Dirac or Weyl semimetal and unconventional superconductivity [1–7]. Recently, a new family of quasi-two-dimensional kagome metals AV<sub>3</sub>Sb<sub>5</sub> (*A* = K, Rb, Cs) has been discovered, consisting of perfect kagome lattice of V atoms coordinated by Sb [8]. Nonmagnetic AV<sub>3</sub>Sb<sub>5</sub> goes through a CDW transition at 78–103 K, then enters the superconducting state below  $T_C \sim 0.9 - 3.5$  K [8–11]. An electronic structure with several Dirac-cone-like bands, flat band, and topological nontrivial surface states close to the Fermi level, was predicted by theory and then confirmed by angle-resolved photoemission spectroscopy (ARPES) studies [8–12]. A scanning tunneling microscopy (STM) study found that the CDW order is topologically nontrivial with chiral anisotropy [13], which may be responsible for observations of large anomalous Hall effect [14,15].

Superconductivity in AV<sub>3</sub>Sb<sub>5</sub> was predicted to be unconventional [16]. Various experiments showed double superconducting domes under pressure, possible signatures of spin-triplet pairing and an edge supercurrent were observed in Nb/K<sub>1-x</sub>V<sub>3</sub>Sb<sub>5</sub> devices [17–21]. Ultralow

temperature thermal conductivity measurements suggest nodal superconductivity in CsV<sub>3</sub>Sb<sub>5</sub> [18], although magnetic penetration depth experiments manifest nodeless superconductivity [22]. V-shaped superconducting gaps and possible roton pair density wave were observed by STM studies [23,24]. More intriguingly, topological nontrivial surface states were predicted, and thus topological superconductivity was suggested due to the superconducting proximity effect [9,10,12]. The possible appearance of a Majorana zero mode was argued [23]. These studies imply rich physics in the superconducting state of AV<sub>3</sub>Sb<sub>5</sub>, but some of them are controversial and the nature of the superconductivity is still largely elusive. In this Letter, we systematically studied the superconducting state of CsV<sub>3</sub>Sb<sub>5</sub>, and found direct evidence and critical clues on the *s*-wave superconducting pairing symmetry, multiband superconductivity and its band-dependent gap distribution, and band-dependent interactions with CDW orders.

CsV<sub>3</sub>Sb<sub>5</sub> crystallizes in a layered structure of V-Sb sheets intercalated by a hexagonal Cs layer [Fig. 1(a)]. The V-Sb sheets consist of a V kagome sublattice, a hexagonal Sb2 sublattice centered on each kagome hexagon, and a honeycomb Sb1 sublattice below and above each kagome layer [Fig. 1(b)]. CsV<sub>3</sub>Sb<sub>5</sub> single crystals with a  $T_C$  of 2.6 K [Fig. S1 in Supplemental Material (SM,

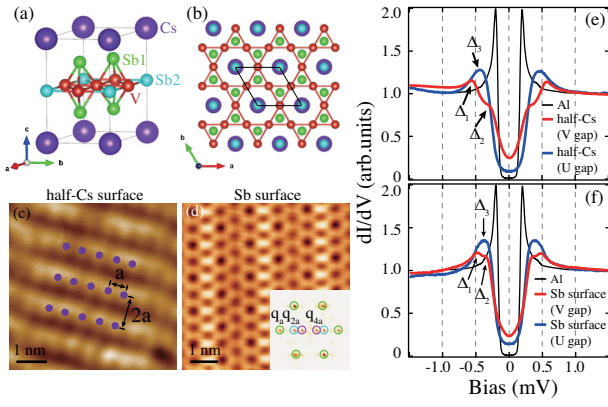


FIG. 1. Typical STM images and superconducting spectra of  $\text{CsV}_3\text{Sb}_5$ . (a),(b) Crystal structure of  $\text{CsV}_3\text{Sb}_5$ . (c),(d) STM images of half-Cs ( $V_b = 200$  mV,  $I_t = 60$  pA) and Sb surfaces ( $V_b = 70$  mV,  $I_t = 209$  pA). The  $1 \times 2$  reconstruction of Cs atoms is sketched in panel (c). Inset of panel (d) shows FFT image of Sb surface, with  $q_a$ ,  $q_{2a}$ , and  $q_{4a}$  spots marked by green, cyan, and magenta circles, respectively. (e),(f) Two kinds of superconducting spectra measured on half-Cs and Sb surfaces, normalized by the  $dI/dV$  value at  $V_b = 1.5$  mV (set point:  $V_b = 1.20$  mV,  $I_t = 150$  pA,  $\Delta V = 30$   $\mu\text{V}$ ). Superconducting spectrum of Al polycrystal ( $T_C \sim 1.2$  K) measured in the same setup is displayed for comparison.

Ref. [25]) were studied by a dilution-refrigerator-equipped STM with a base temperature of 40 mK and an effective electron temperature  $T_{\text{eff}}$  of 170 mK (Fig. S2). Two kinds of surface terminations were observed, one is half-Cs surface with Cs atoms forming  $1 \times 2$  reconstructions [Fig. 1(c)], the other is a honeycombed Sb1 surface exhibiting two charge modulations [Fig. 1(d)], one being a  $2a \times 2a$  superstructure propagating along three lattice directions ( $a \sim 5.5$  Å is the lattice period) and the other being a unidirectional  $4a$  modulation. Such charge modulations are resolved more clearly in the fast-Fourier transform (FFT) image in the inset,  $q_{2a}$  and  $q_{4a}$  spots are clearly presented in addition to Bragg peak  $q_a$ . These charge modulations are similar to previous STM studies on  $\text{AV}_3\text{Sb}_5$ , and are assigned to multiple CDW orders [13,23,24,27,28].

On both half-Cs and Sb surfaces, we observed spatially homogeneous superconducting gap spectra, with just small intensity modulations from the CDW (this will be discussed later). However, likely due to different STM tip conditions in different measurements, the superconducting gap spectrum is found to be either V shaped or U shaped on both types of surfaces, as shown in Figs. 1(e) and 1(f) (more details are elaborated in Sec. 3 of SM). The V-shaped superconducting gap on Sb surface [Fig. 1(f)] exhibits two pairs of coherence peaks located at  $\Delta_1 = 0.48$  meV and  $\Delta_2 = 0.36$  meV, and its gap depth [defined by  $1-N(0)$ , where  $N(0)$  is the normalized  $dI/dV$  value at zero energy] is 75%  $\sim$  80%; while the U-shaped superconducting gap has a pair of broad coherence peaks at about

$\Delta_3 = 0.38$  meV and a rather flat bottom with the gap depth of about 90%. For half-Cs surfaces, similar V- and U-shaped superconducting gaps are observed [Fig. 1(e)], but the gap sizes differ slightly ( $\Delta_1 = 0.57$  meV,  $\Delta_2 = 0.30$  meV and  $\Delta_3 = 0.45$  meV). For comparison, the superconducting gap of Al ( $T_C \sim 1.2$  K) measured at the same condition displays a flat bottom with zero DOS [black curves in Figs. 1(e) and 1(f)]. This confirms the existence of residual DOS in the superconducting gap of  $\text{CsV}_3\text{Sb}_5$  (see Fig. S6 for more details). Considering the multiband nature of  $\text{AV}_3\text{Sb}_5$  [8–12], the different superconducting gaps may originate from different bands. Their appearance depends on specific tip states, which results in different tunneling probabilities for different bands. Because the half-Cs surface is unstable due to the high mobility of Cs atoms and low coverage (Fig. S7), we will mainly focus on Sb surfaces hereafter.

Superconductivity of  $\text{CsV}_3\text{Sb}_5$  is further investigated by imaging magnetic vortices. Figures 2(a) and 2(b) show vortex maps on Sb surface with U-shaped superconducting gaps. The vortices form a perfect Abrikosov lattice, but a single vortex is anisotropic and exhibits a sixfold star-shaped structure. Such anisotropic vortex is generally believed to arise from anisotropic multiband nature of the Fermi surfaces and/or superconducting pairing symmetry, as reported in  $\text{NbSe}_2$ ,  $\text{YNi}_2\text{B}_2\text{C}$ ,  $\text{LiFeAs}$  [29–33].

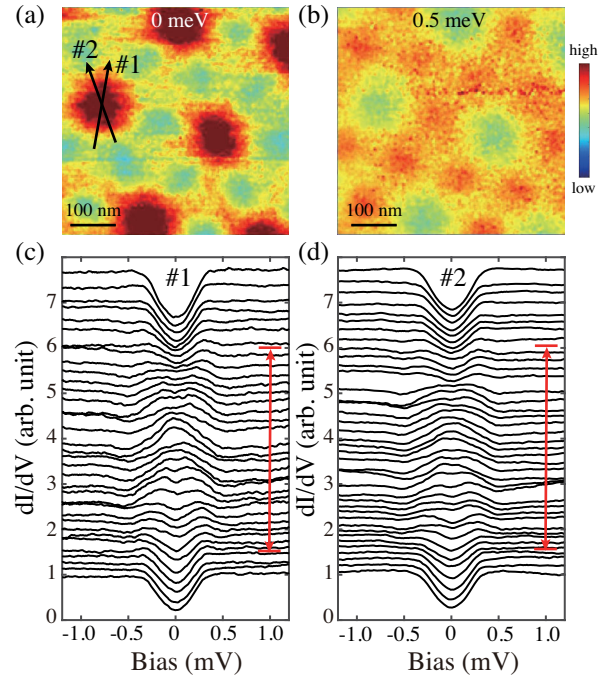


FIG. 2. Vortex states measured on the Sb surface. (a),(b) Vortex maps at 0 and 0.5 meV under  $B_{\perp} = 500$  Oe ( $V_b = 1.20$  mV,  $I_t = 100$  pA,  $\Delta V = 30$   $\mu\text{V}$ ). (c),(d) Evolution of  $dI/dV$  spectra taken along cuts No. 1 and No. 2 in panel (a) ( $V_b = 1.20$  mV,  $I_t = 150$  pA,  $\Delta V = 30$   $\mu\text{V}$ ). The red bidirectional arrows indicate the  $\pm 40$  nm area away from the vortex core.

The reported twofold symmetric superconductivity by transport measurements is not evidenced in the vortex structure here [34,35]. Figures 2(c) and 2(d) show the evolution of  $dI/dV$  spectra across a vortex core, taken along linecuts No. 1 and No. 2 in Fig. 2(a). Upon approaching the vortex core, the superconducting gap is gradually suppressed. At a distance of about  $\pm 40$  nm away from the vortex core, a pair of broad peaks inside the superconducting gap appears, and their energy separation decreases gradually upon approaching the vortex core. These two peaks are discernible at 10 nm away from the vortex core, but merge into a broad asymmetric peak near the vortex center. Similar results have been observed in vortices on all Sb and Cs surfaces, no matter V- or U-shaped gap is observed in the absence of magnetic field (Fig. S8). The evolution of vortex states is consistent with conventional Caroli–de Gennes–Matricon (CdGM) bound states [36].  $\text{CsV}_3\text{Sb}_5$  possesses multiple Fermi pockets with Fermi energy ( $E_F$ ) of about 50–700 meV [12]. By using the observed largest superconducting gap  $\Delta_3 \sim 0.57$  meV, the estimated upper limit of the energy separation of the CdGM bound states  $\delta E = \Delta^2/E_F$  (Ref. [36]) is about  $6.5 \mu\text{eV}$ , thus the CdGM states of different bands cannot be distinguished in our STM study and appear as a broad peak containing multiple CdGM states.

To further explore the superconducting gap structure, impurity effects are studied. The response of superconductivity to local impurities generally depends on the pairing symmetry and the nature of the impurities [37]. It is known that for  $s$ -wave pairing, only magnetic impurities can break the Cooper pair and induce in-gap bound states [38]. However, for sign-changing pairing functions such as  $d$ -wave and  $s_{\pm}$ -wave, nonmagnetic impurities with proper scattering potentials can also induce in-gap states and suppress superconductivity [39–44].

We investigate the impurity effects of superconductivity in  $\text{CsV}_3\text{Sb}_5$  by studying the intrinsic defects, as well as artificially introduced impurities. Insets of Figs. 3(a) and 3(b) show two intrinsic holelike defects located at Sb1 site and V site underneath that are assigned as a Sb1 vacancy and a V defect. The superconducting gap is unaffected at both defects and their vicinity, and no in-gap states are observed [Figs. 3(a) and 3(b)]. Since no signature of magnetic order or local magnetic moment was observed in  $\text{CsV}_3\text{Sb}_5$  [8,45], these intrinsic defects are considered to be nonmagnetic. Similarly, nonmagnetic Cs adatom does not affect the superconductivity [Fig. 3(c)]. Besides, nonmagnetic Zn atoms and magnetic Cr atoms were evaporated separately onto the sample kept at about 30 K, and appear as bright protrusions [insets of Figs. 3(d) and 3(e)]. Assuming that the interaction between low-temperature adsorbed atoms and underlying lattice is weak, the impurity atoms are expected to retain their nonmagnetic or magnetic character after adsorption. For Zn adatoms, the superconducting gap remains unchanged at the Zn site and its vicinity. While for the Cr cluster, the superconducting gap is greatly suppressed, and a pair of asymmetric peaks appear inside the gap. These are hallmarks of impurity-induced in-gap states. Away from the Cr cluster, the impurity states are weakened, and the superconducting gap gradually recovers. Overall, the magnetic Cr cluster strongly suppresses the superconductivity of  $\text{CsV}_3\text{Sb}_5$  while the nonmagnetic impurities not, clearly indicating that there is no sign change in the superconducting pairing function of  $\text{CsV}_3\text{Sb}_5$ .

The interplay between multiband superconductivity and CDWs is manifested in the spatial DOS modulation of V- and U-shaped superconducting gaps. Figures 4(a)–4(d) and Figs. S9 show DOS maps and corresponding FFTs at various energies for the V-shaped gap, taken in the Sb

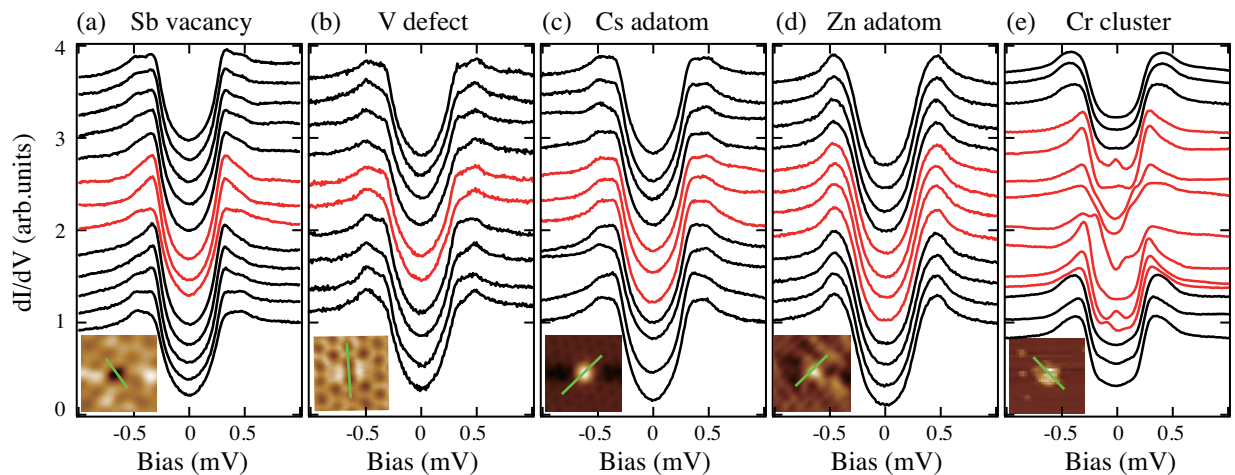


FIG. 3. Impurity effects on the superconductivity of  $\text{CsV}_3\text{Sb}_5$ . Series of  $dI/dV$  spectra taken along the linecuts (green lines in the insets) across various defects and adatoms. STM images of these defects and adatoms are displayed in the insets. The red curves are collected near the center of the defects and adatoms.

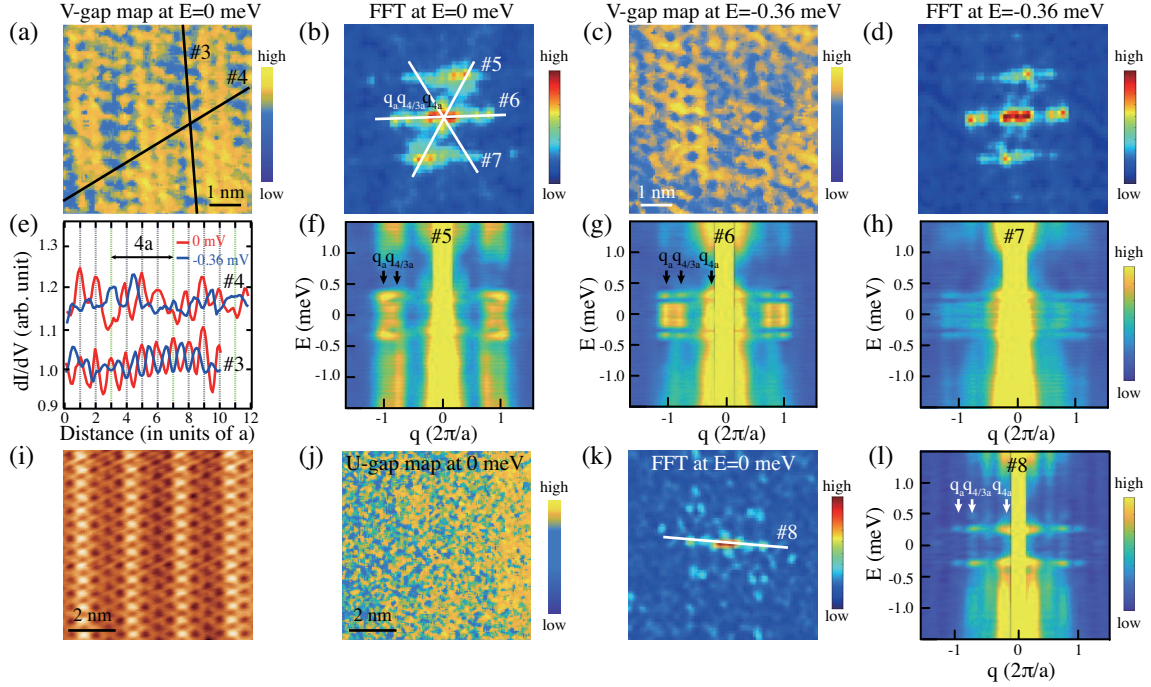


FIG. 4. Spatial DOS modulations for V-shaped (a)–(h) and U-shaped (i)–(l) superconducting gaps on Sb surface. (a)–(d) DOS maps ( $V_b = 1.20$  mV,  $I_t = 300$  pA,  $\Delta V = 30$   $\mu$ V) and corresponding FFTs under  $E = 0$  meV and  $-0.36$  meV, taken in the region shown in Fig. 1(d). (e) Comparison of spatial DOS modulations under  $E = 0$  meV and  $-0.36$  meV, taken along cuts No. 3 and No. 4 in panel (a). (f)–(h) Color plots of FFT linecuts along No. 5–No. 7 directions in panel (b). (i) Atomically resolved STM image of a Sb surface with U-shaped gap ( $V_b = 50$  mV,  $I_t = 200$  pA), and corresponding DOS map (j) and FFT (k) under  $E = 0$  meV ( $V_b = 1.20$  mV,  $I_t = 200$  pA,  $\Delta V = 30$   $\mu$ V). (l) Color plot of FFT linecut along No. 8 direction in panel (k).

surface shown in Fig. 1(d). Obvious spatial modulations are resolved, the spatial dependencies of DOSs at zero energy and the coherence peak energy ( $E = -0.36$  meV) measured along two lattice directions [cuts No. 3 and No. 4 in Fig. 4(a)] are displayed in Fig. 4(e). Along cut No. 3 without  $4a$  CDW, the DOSs at these two energies oscillate at a period of  $a$  and are out of phase. Such antiphase behavior is consistent with the superconducting picture that a higher coherence peak is concomitant with a lower residual DOS at zero energy, and suggests the observed DOS modulation is intrinsic to superconducting state, instead of the influence of atomic Bragg oscillations (Fig. S10). Along cut No. 4 with  $4a$  CDW, the minimal oscillation period is still  $a$ , but the oscillation intensity is strongly influenced by  $4a$  CDW and shows additional  $4a$  period. Figures 4(f)–4(h) show the energy dependencies of these DOS modulations, taken along cuts No. 5–7 in Fig. 4(b).  $q_a$  and  $q_{4a}$  spots are nondispersive but show strong spatial anisotropy; they are weaker around the coherence peak energy, suggesting the competition between these modulations and the homogeneous superconductivity. As for U-shaped superconducting gap, although  $2a \times 2a$  and  $4a$  CDWs are also present in STM image [Fig. 4(i)], the DOS modulation is weak and the influence of CDWs is not obvious except for those near the coherence peak energies [Figs. 4(j)–4(l) and Fig. S11]. These discrepancies indicate

that the interactions between CDWs and different superconducting gaps are different.

Finally, we discuss the superconducting pairing symmetry of  $\text{CsV}_3\text{Sb}_5$  and origin of the observed complex superconducting spectra. Absence of sign change indicated by impurity effects suggests an  $s$ -wave superconducting pairing symmetry. It can exclude exotic superconducting pairing symmetries with sign-change order parameters [5,16], and is consistent with the decrease of Knight shift and a Hebel-Slichter coherence peak in  $1/T_1T$  just below  $T_C$  in recent nuclear magnetic resonance studies [46]. However, the finite residual DOS at Fermi level observed in our data, together with the finite thermal conductivity measured down to 100 mK nominal-lattice temperature [18], seem to suggest either the existence of gap nodes, or extremely small but full superconducting gaps in certain Fermi surface sections that are still partially filled at  $T_{\text{eff}} \sim 170$  mK in our apparatus. Considering the absence of sign change, the latter case seems to be more likely than the appearance of accidental gap nodes.

$\text{CsV}_3\text{Sb}_5$  is a multiband system with multiple Fermi surface sheets. The Sb- $p$  orbital contributes a circular electron pocket at  $\Gamma$ , while the V- $d$  orbitals form multiple sizable triangular electron pockets at  $K$  and saddle points with high DOS at  $M$  [12,27]. In particular, several tiny oval pockets near  $K$  and  $M$  are revealed by quantum oscillation

measurements [47,48]. Its CDW gap is strongly momentum and band dependent according to theoretical and ARPES studies. It is the largest around  $M$ , and anisotropic on the pockets around  $K$  with zero gap along the  $\Gamma$ - $K$  direction, and it is absent around the  $\Gamma$  Fermi pocket [49–51]. Interestingly, similar to the cases of 2H-NbSe<sub>2</sub> and 2H-Na<sub>x</sub>TaS<sub>2</sub> [52,53], the Fermi surface is only *partially* gapped when there is a CDW gap, probably due to the strong coupling nature of electron-phonon interactions. This implies that both CDW and superconductivity compete on the same spectral weight near the Fermi energy. Since CDW occurs at higher temperature with larger energy scale, the presence of CDW gaps would affect the superconducting pairing behavior and alter the superconducting gap distribution. Moreover, because the tunneling matrix elements of the states on a particular Fermi pocket depend on the wave function distributions of these states and that of the STM tip [54], the superconducting gap at different Fermi pockets may be preferentially probed in different measurements with different tip conditions. Consistently, the distinct line shapes of the two superconducting gaps, especially near the gap bottom, and their responses to CDWs in Fig. 4, suggest that they are originated from different Fermi pockets with different CDW behaviors. Therefore, based on our data and the recent ARPES data of the CDW gap, one can deduce the following picture: (1) the V-shaped superconducting gap corresponds to strongly anisotropic gap distribution, which probably originates from the triangular Fermi pockets or sections around  $K$  with anisotropic CDW gaps. In these pockets, the effects of CDW are strong, therefore, the competition between CDW and superconductivity is strongly present (Fig. 4), resulting in an anisotropic superconducting gap. (2) The U-shaped gap corresponds to a more isotropic superconducting gap, and thus is more likely derived from the circular electron pocket at  $\Gamma$ , which is little affected by the CDW. (3) Some extremely small but full superconducting gaps might locate at the aforementioned tiny oval pockets near  $K$  and  $M$  [47,48], on which weak superconducting pairing is expected. These tiny pockets could contribute a small residual DOS at zero energy even at  $T_{\text{eff}} \sim 170$  mK, which puts an upper limit of about 0.05 meV ( $\sim 3k_B T_{\text{eff}}$ ) to the superconducting gap there.

In summary, we systematically studied the superconductivity of CsV<sub>3</sub>Sb<sub>5</sub> by using an ultralow temperature STM with high energy and spatial resolution. Our results indicate an *s*-wave superconducting pairing symmetry, and that the superconductivity has band-dependent gap functions, and band-dependent interplay with CDW orders, which facilitate further understanding of the complex entanglements of superconductivity, topology, and charge order in kagome compounds.

We thank Yilin Wang, Juan Jiang, Tong Zhang, and Shiyang Li for helpful discussions. Measurements of magnetic and electrical properties were conducted on the <sup>3</sup>He

insert of MPMS3 and PPMS at Instruments Center for Physical Science of University of Science and Technology of China. This work is supported by the National Natural Science Foundation of China (Grants No. 12074363, No. 11790312, No. 11888101, No. 11774060 and No. 92065201), National Key R&D Program of the MOST of China (Grants No. 2017YFA0303004, No. 2016YFA0300200, and No. 2017YFA0303104).

\*Corresponding author.

yanyj87@ustc.edu.cn

†Corresponding author.

dlfeng@ustc.edu.cn

- [1] L. D. Ye, M. G. Kang, J. W. Liu, F. V. Cube, C. R. Wicker, T. Suzuki, C. Jozwiak, A. Bostwick, E. Rotenberg, D. C. Bell, L. Fu, R. Comin, and J. G. Checkelsky, Massive Dirac fermions in a ferromagnetic kagome metal, *Nature (London)* **555**, 638 (2018).
- [2] J.-X. Yin, S. S. Zhang, G. Q. Chang, Q. Wang, S. S. Tsirkin, Z. Guguchia, B. Lian, H. B. Zhou, K. Jiang, I. Belopolski, N. Shumiya, D. Multer, M. Litskevich, T. A. Cochran, H. Lin, Z. Q. Wang, T. Neupert, S. Jia, H. C. Lei, and M. Z. Hasan, Negative flat band magnetism in a spin-orbit-coupled correlated kagome magnet, *Nat. Phys.* **15**, 443 (2019).
- [3] L. Balents, Spin liquids in frustrated magnets, *Nature (London)* **464**, 199 (2010).
- [4] W.-H. Ko, P. A. Lee, and X.-G. Wen, Doped kagome system as exotic superconductor, *Phys. Rev. B* **79**, 214502 (2009).
- [5] S.-L. Yu and J.-X. Li, Chiral superconducting phase and chiral spin-density-wave phase in a Hubbard model on the kagome lattice, *Phys. Rev. B* **85**, 144402 (2012).
- [6] W.-S. Wang, Z.-Z. Li, Y.-Y. Xiang, and Q.-H. Wang, Competing electronic orders on kagome lattices at van Hove filling, *Phys. Rev. B* **87**, 115135 (2013).
- [7] M. L. Kiesel, C. Platt, and R. Thomale, Unconventional Fermi Surface Instabilities in the Kagome Hubbard Model, *Phys. Rev. Lett.* **110**, 126405 (2013).
- [8] B. R. Ortiz, L. C. Gomes, J. R. Morey, M. Winiarski, M. Bordelon, J. S. Mangum, I. W. H. Oswald, J. A. Rodriguez-Rivera, J. R. Neilson, S. D. Wilson, E. Ertekin, T. M. McQueen, and E. S. Toberer, New kagome prototype materials: Discovery of KV<sub>3</sub>Sb<sub>5</sub>, RbV<sub>3</sub>Sb<sub>5</sub>, and CsV<sub>3</sub>Sb<sub>5</sub>, *Phys. Rev. Mater.* **3**, 094407 (2019).
- [9] B. R. Ortiz, S. M. L. Teicher, Y. Hu, J. L. Zuo, P. M. Sarte, E. C. Schueller, A. M. M. Abeykoon, M. J. Krogstad, S. Rosenkranz, R. Osborn, R. Seshadri, L. Balents, J. F. He, and S. D. Wilson, CsV<sub>3</sub>Sb<sub>5</sub>: A  $\mathbb{Z}_2$  Topological Kagome Metal with a Superconducting Ground State, *Phys. Rev. Lett.* **125**, 247002 (2020).
- [10] B. R. Ortiz, P. M. Sarte, E. M. Kenney, M. J. Graf, S. M. L. Teicher, R. Seshadri, and S. D. Wilson, Superconductivity in the  $\mathbb{Z}_2$  kagome metal KV<sub>3</sub>Sb<sub>5</sub>, *Phys. Rev. Mater.* **5**, 034801 (2021).
- [11] Q. W. Yin, Z. J. Tu, C. S. Gong, Y. Fu, S. H. Yan, and H. C. Lei, Superconductivity and normal-state properties of kagome metal RbV<sub>3</sub>Sb<sub>5</sub> single crystals, *Chin. Phys. Lett.* **38**, 037403 (2021).

- [12] Z. H. Liu, N. N. Zhao, Q. W. Yin, C. S. Gong, Z. J. Tu, M. Li, W. H. Song, Z. T. Liu, D. W. Shen, Y. B. Huang, K. Liu, H. C. Lei, and S. C. Wang, Temperature-induced band renormalization and Lifshitz transition in a kagome superconductor  $\text{RbV}_3\text{Sb}_5$ , [arXiv:2104.01125](https://arxiv.org/abs/2104.01125).
- [13] Y.-X. Jiang *et al.*, Unconventional chiral charge order in kagome superconductor  $\text{KV}_3\text{Sb}_5$ , *Nat. Mater.* **20**, 1353 (2021).
- [14] S.-Y. Yang, Y. Wang, B. R. Ortiz, D. Liu, J. Gayles, E. Derunova, R. Gonzalez-Hernandez, L. Šmejkal, Y. L. Chen, S. S. P. Parkin, S. D. Wilson, E. S. Toberer, T. McQueen, and M. N. Ali, Giant, unconventional anomalous Hall effect in the metallic frustrated magnet candidate  $\text{KV}_3\text{Sb}_5$ , *Sci. Adv.* **6**, eabb6003 (2020).
- [15] F. H. Yu, T. Wu, Z. Y. Wang, B. Lei, W. Z. Zhuo, J. J. Ying, and X. H. Chen, Concurrence of anomalous Hall effect and charge density wave in a superconducting topological kagome metal, *Phys. Rev. B* **104**, L041103 (2021).
- [16] X. X. Wu, T. Schwemmer, T. Müller, A. Consiglio, G. Sangiovanni, D. D. Sante, Y. Iqbal, W. Hanke, A. P. Schnyder, M. M. Denner, M. H. Fischer, T. Neupert, and R. Thomale, Nature of unconventional pairing in the kagome superconductors  $\text{AV}_3\text{Sb}_5$ , [arXiv:2104.05671](https://arxiv.org/abs/2104.05671).
- [17] Y. J. Wang, S. Y. Yang, P. K. Sivakumar, B. R. Ortiz, S. M. L. Teicher, H. Wu, A. K. Srivastava, C. Garg, D. F. Liu, S. S. P. Parkin, E. S. Toberer, T. McQueen, S. D. Wilson, and M. N. Ali, Proximity-induced spin-triplet superconductivity and edge supercurrent in the topological kagome metal,  $\text{K}_{1-x}\text{V}_3\text{Sb}_5$ , [arXiv:2012.05898](https://arxiv.org/abs/2012.05898).
- [18] C. C. Zhao, L. S. Wang, W. Xia, Q. W. Yin, J. M. Ni, Y. Y. Huang, C. P. Tu, Z. C. Tao, Z. J. Tu, C. S. Gong, H. C. Lei, Y. F. Guo, X. F. Yang, and S. Y. Li, Nodal superconductivity and superconducting domes in the topological kagome metal  $\text{CsV}_3\text{Sb}_5$ , [arXiv:2102.08356](https://arxiv.org/abs/2102.08356).
- [19] K. Y. Chen, N. N. Wang, Q. W. Yin, Y. H. Gu, K. Jiang, Z. J. Tu, C. S. Gong, Y. Uwatoko, J. P. Sun, H. C. Lei, Y. Uwatoko, and J.-G. Cheng, Double superconducting dome and triple enhancement of  $T_C$  in the kagome superconductor  $\text{CsV}_3\text{Sb}_5$  under high pressure, *Phys. Rev. Lett.* **126**, 247001 (2021).
- [20] F. Du, S. S. Luo, B. R. Ortiz, Y. Chen, W. Y. Duan, D. T. Zhang, X. Lu, S. D. Wilson, Y. Song, and H. Q. Yuan, Pressure-induced double superconducting domes and charge instability in the kagome metal  $\text{KV}_3\text{Sb}_5$ , *Phys. Rev. B* **103**, L220504 (2021).
- [21] Z. Y. Zhang, Z. Chen, Y. Zhou, Y. F. Yuan, S. Y. Wang, L. L. Zhang, X. D. Zhu, Y. H. Zhou, X. L. Chen, J. H. Zhou, and Z. R. Yang, Pressure-induced reemergence of superconductivity in topological kagome metal  $\text{CsV}_3\text{Sb}_5$ , *Phys. Rev. B* **103**, 224513 (2021).
- [22] W. Y. Duan, Z. Y. Nie, S. S. Luo, F. H. Yu, B. R. Ortiz, L. C. Yin, H. Su, F. Du, A. Wang, Y. Chen, X. Lu, J. J. Ying, S. D. Wilson, X. H. Chen, Y. Song, and H. Q. Yuan, Nodeless superconductivity in the kagome metal  $\text{CsV}_3\text{Sb}_5$ , *Sci. China-Phys. Mech. Astron.* **64**, 107462 (2021).
- [23] Z. W. Liang, X. Y. Hou, F. Zhang, W. R. Ma, W. R. Ma, F. Zhang, P. Wu, Z. Y. Zhang, F. H. Yu, J.-J. Ying, K. Jiang, L. Shan, Z. Y. Wang, and X.-H. Chen, Three-dimensional charge density wave and robust zero-bias conductance peak inside the superconducting vortex core of a kagome superconductor  $\text{CsV}_3\text{Sb}_5$ , *Phys. Rev. X* **11**, 031026 (2021).
- [24] H. Chen *et al.*, Roton pair density wave in a strong-coupling kagome superconductor, *Nature (London)* (2021), <https://doi.org/10.1038/s41586-021-03983-5>.
- [25] See Supplemental Material at <http://link.aps.org/supplemental/10.1103/PhysRevLett.127.187004> for Figs. S1–S11, which includes Refs. [8,26].
- [26] P. O. Sprau, A. Kostin, A. Kreise, A. E. Böhmer, V. Taufour, P. C. Canfield, S. Mukherjee, P. J. Hirschfeld, B. M. Andersen, and J. C. Séamus Davis, Discovery of orbital-selective Cooper pairing in  $\text{FeSe}$ , *Science* **357**, 75 (2017).
- [27] H. Zhao, H. Li, B. R. Ortiz, S. M. L. Teicher, T. Park, M. X. Ye, Z. Q. Wang, L. Balents, S. D. Wilson, and I. Zeljkovic, Cascade of correlated electron states in a kagome superconductor  $\text{CsV}_3\text{Sb}_5$ , *Nature (London)* (2021), <https://doi.org/10.1038/s41586-021-03946-w>.
- [28] H. X. Tan, Y. Z. Liu, Z. Q. Wang, and B. H. Yan, Charge density waves and electronic properties of superconducting kagome metals, *Phys. Rev. Lett.* **127**, 046401 (2021).
- [29] H. F. Hess, R. B. Robinson, and J. V. Waszczak, Vortex-Core Structure Observed with a Scanning Tunneling Microscope, *Phys. Rev. Lett.* **64**, 2711 (1990).
- [30] H. Nishimori, K. Uchiyama, S.-i. Kaneko, A. Tokura, H. Takeya, K. Hirata, and N. Nishida, First observation of the fourfold-symmetric and quantum regime vortex core in  $\text{YNi}_2\text{B}_2\text{C}$  by scanning tunneling microscopy and spectroscopy, *J. Phys. Soc. Jpn.* **73**, 3247 (2004).
- [31] T. Hanaguri, K. Kitagawa, K. Matsubayashi, Y. Mazaki, Y. Uwatoko, and H. Takagi, Scanning tunneling microscopy/spectroscopy of vortices in  $\text{LiFeAs}$ , *Phys. Rev. B* **85**, 214505 (2012).
- [32] N. Hayashi, M. Ichioka, and K. Machida, Star-Shaped Local Density of States around Vortices in a Type-II Superconductor, *Phys. Rev. Lett.* **77**, 4074 (1996).
- [33] N. Hayashi, M. Ichioka, and K. Machida, Effects of gap anisotropy upon the electronic structure around a superconducting vortex, *Phys. Rev. B* **56**, 9052 (1997).
- [34] S. L. Ni *et al.*, Anisotropic superconducting properties of kagome metal  $\text{CsV}_3\text{Sb}_5$ , *Chin. Phys. Lett.* **38**, 057403 (2021).
- [35] Y. Xiang, Q. Li, Y. K. Li, W. Xie, H. Yang, Z. W. Wang, Y. G. Yao, and H.-H. Wen, Nematic electronic state and twofold symmetry of superconductivity in the topological kagome metal  $\text{CsV}_3\text{Sb}_5$ , [arXiv:2104.06909](https://arxiv.org/abs/2104.06909).
- [36] C. Caroli, P. G. De Gennes, and J. Matricon, Bound fermion states on a vortex line in a type ii superconductor, *Phys. Lett.* **9**, 307 (1964).
- [37] A. V. Balatsky, I. Vekhter, and J.-X. Zhu, Impurity-induced states in conventional and unconventional superconductors, *Rev. Mod. Phys.* **78**, 373 (2006).
- [38] P. W. Anderson, Theory of dirty superconductors, *J. Phys. Chem. Solids* **11**, 26 (1959).
- [39] S. Onari and H. Kontani, Violation of Anderson's Theorem for the Sign-Reversing  $s$ -Wave State of Iron-Pnictide Superconductors, *Phys. Rev. Lett.* **103**, 177001 (2009).
- [40] D. Zhang, Nonmagnetic Impurity Resonances as a Signature of Sign-Reversal Pairing in  $\text{FeAs}$ -Based Superconductors, *Phys. Rev. Lett.* **103**, 186402 (2009).

- [41] T. Kariyado and M. Ogata, Single-impurity problem in iron-pnictide superconductors, *J. Phys. Soc. Jpn.* **79**, 083704 (2010).
- [42] S. H. Pan, E. W. Hudson, K. M. Lang, H. Eisaki, S. Uchida, and J. C. Davis, Imaging the effects of individual zinc impurity atoms on superconductivity in  $\text{Bi}_2\text{Sr}_2\text{CaCu}_2\text{O}_{8+\delta}$ , *Nature (London)* **403**, 746 (2000).
- [43] H. Yang, Z. Y. Wang, D. L. Fang, Q. Deng, Q. H. Wang, Y. Y. Xiang, Y. Yang, and H. H. Wen, In-gap quasiparticle excitations induced by non-magnetic Cu impurities in  $\text{Na}(\text{Fe}_{0.96}\text{Co}_{0.03}\text{Cu}_{0.01})\text{As}$  revealed by scanning tunnelling spectroscopy, *Nat. Commun.* **4**, 2749 (2013).
- [44] S. Grothe, S. Chi, P. Dosanjh, R. X. Liang, W. N. Hardy, S. A. Burke, D. A. Bonn, and Y. Pennec, Bound states of defects in superconducting  $\text{LiFeAs}$  studied by scanning tunneling spectroscopy, *Phys. Rev. B* **86**, 174503 (2012).
- [45] E. M. Kenney, B. R. Ortiz, C. N. Wang, S. D. Wilson, and M. J. Graf, Absence of local moments in the kagome metal  $\text{KV}_3\text{Sb}_5$  as determined by muon spin spectroscopy, *J. Phys. Condens. Matter* **33**, 235801 (2021).
- [46] C. Mu, Q. W. Yin, Z. J. Tu, C. S. Gong, H. C. Lei, Z. Li, and J. L. Luo, *s*-wave superconductivity in kagome metal  $\text{CsV}_3\text{Sb}_5$  revealed by  $^{121/123}\text{Sb}$  NQR and  $^{51}\text{V}$  NMR measurements, *Chin. Phys. Lett.* **38**, 077402 (2021).
- [47] B. R. Ortiz, S. M. L. Teicher, L. Kautzsch, P. M. Sarte, J. P. C. Ruff, R. Seshadri, and S. D. Wilson, Fermi surface mapping and the nature of charge density wave order in the kagome superconductor  $\text{CsV}_3\text{Sb}_5$ , [arXiv:2104.07230](https://arxiv.org/abs/2104.07230).
- [48] Y. Fu, N. N. Zhao, Z. Chen, Q. W. Yin, Z. J. Tu, C. S. Gong, C. Y. Xi, X. D. Zhu, Y. P. Sun, K. Liu, and H. C. Lei, Quantum transport evidence of topological band structures of kagome superconductor  $\text{CsV}_3\text{Sb}_5$ , [arXiv:2104.08193](https://arxiv.org/abs/2104.08193).
- [49] M. M. Denner, R. Thomale, and T. Neupert, Analysis of charge order in the kagome metal  $\text{AV}_3\text{Sb}_5$  ( $A = \text{K}, \text{Rb}, \text{Cs}$ ), [arXiv:2103.14045](https://arxiv.org/abs/2103.14045).
- [50] Z. G. Wang, S. Ma, Y. H. Zhang, H. T. Yang, Z. Zhao, Y. Ou, Y. Zhu, S. L. Ni, Z. Y. W. Lu, H. Chen, K. Jiang, L. Yu, Y. Zhang, X. L. Dong, J. P. Hu, H.-J. Gao, and Z. X. Zhao, Distinctive momentum dependent charge-density-wave gap observed in  $\text{CsV}_3\text{Sb}_5$  superconductor with topological kagome lattice, [arXiv:2104.05556](https://arxiv.org/abs/2104.05556).
- [51] K. Nakayama, Y. K. Li, M. Liu, Z. W. Wang, T. Takahashi, Y. G. Yao, and T. Sato, Multiple energy scales and anisotropic energy gap in the charge-density-wave phase of kagome superconductor  $\text{CsV}_3\text{Sb}_5$ , [arXiv:2104.08042](https://arxiv.org/abs/2104.08042).
- [52] D. W. Shen, Y. Zhang, L. X. Yang, J. Wei, H. W. Ou, J. K. Dong, C. He, B. P. Xie, J. F. Zhao, B. Zhou, M. Arita, K. Shimada, H. Namatame, M. Taniguchi, J. Shi, and D. L. Feng, Primary Role of the Barely Occupied States in the Charge Density Wave Formation of  $\text{NbSe}_2$ , *Phys. Rev. Lett.* **101**, 226406 (2008).
- [53] D. W. Shen, B. P. Xie, J. F. Zhao, L. X. Yang, L. Fang, J. Shi, R. H. He, D. H. Lu, H. H. Wen, and D. L. Feng, Novel Mechanism of a Charge Density Wave in a Transition Metal Dichalcogenide, *Phys. Rev. Lett.* **99**, 216404 (2007).
- [54] Y. Noat, J. A. Silva-Guillén, T. Cren, V. Cherkez, C. Brun, S. Pons, F. Debontridder, D. Roditchev, W. Sacks, L. Cario, P. Ordejón, A. García, and E. Canadell, Quasiparticle spectra of  $2\text{H-NbSe}_2$ : Two-band superconductivity and the role of tunneling selectivity, *Phys. Rev. B* **92**, 134510 (2015).